Foucher, C. and Guilhabert, B. and Herrnsdorf, J. and Laurand, N. and Dawson, M. D. (2014) Diode-pumped, mechanically-flexible polymer DFB laser encapsulated by glass membranes. Optics Express, 22 (20). pp. 24160-24168. ISSN 1094-4087 , http://dx.doi.org/10.1364/OE.22.024160

Diode-pumped, mechanically-flexible polymer DFB laser encapsulated by glass membranes

C. Foucher,[1*] B. Guilhabert,[1] J. Herrnsdorf,[1] N. Laurand,[1] and M.D. Dawson[1]

[1]*Institute of Photonics, University of Strathclyde, Glasgow G4 0NW, UK*

[*]caroline.foucher@strath.ac.uk

Abstract: A diode-pumped, mechanically-flexible organic distributed-feedback laser that is fully encapsulated with ultra-thin glass is reported. The organic laser is excited by 450nm laser diode and emits at 537 nm with an oscillation threshold of 290 W/cm^2. The encapsulation format of the device results in a photostability that is improved by two orders of magnitude compared to a non-encapsulated reference device while maintaining mechanical flexibility thanks to an overall device thickness below 105 µm. The laser is also wavelength-tunable between 535 nm and 545 nm by bending the ultra-thin glass structure.

OCIS codes: (140.0140) Lasers and laser optics; (160.4890) Organic materials; (140.3490) Lasers, distributed-feedback.

References and links

1. I.D.W. Samuel, G.A. Turnbull. "Organic semiconductor lasers," Chem. Rev. 107(4), 1272–95 (2007).
2. P. Görrn, M. Lehnhardt, W. Kowalsky, T. Riedl, and S. Wagner. "Elastically tunable self-organized organic lasers," Adv. Mater. 23(7), 869–72 (2011).
3. B. Wenger, N. Tétreault, M.E. Welland, and R.H. Friend. "Mechanically tunable conjugated polymer distributed feedback lasers," Appl. Phys. Lett. 97(19), 193303 (2010).
4. S. Riechel, U. Lemmer, J. Feldmann, T. Benstem, W. Kowalsky, U. Scherf,.A. Gombert, and V. Wittwer "Rapid communication laser modes in organic solid-state distributed feedback lasers," Appl. Phys. Lett. . 900(77), 897–900 (2000).
5. C. Vannahme, C.L.C. Smith, M. Brokner Christiansen, and A. Kristensen. "Emission wavelength of multilayer distributed feedback dye lasers," Appl. Phys. Lett. 101(15), 151123 (2012).
6. M.R. Weinberger, G. Langer, A. Pogantsch, A. Haase, E. Zojer, and W. Kern. "Continuously color-tunable rubber laser," Adv. Mater. 16(2), 130–3. (2004).
7. M.D. McGehee, A. J. Heeger. "Semiconducting (conjugated) polymers as materials for solid-state lasers," Adv. Mater. 12(22), 1655–68 (2000).
8. N. Tessler. "Lasers based on semiconducting organic materials," Adv. Mater. 11(5), 363–70 (1999).
9. C. Pflumm, C. Karnutsch, M. Gerken, and U. Lemmer. "Parametric study of modal gain and threshold power density in electrically pumped single-layer organic optical amplifier and laser diode structures," IEEE J. Quantum Electron. 41(3), 316–36 (2005).
10. Y. Yang, G.A. Turnbull, and I.D.W. Samuel. "Hybrid optoelectronics: A polymer laser pumped by a nitride light-emitting diode," Appl. Phys. Lett. 92(16), 163306 (2008).
11. T. Riedl, T. Rabe, H.-H. Johannes, W. Kowalsky, J. Wang, T. Weimann, P. Hinze, B. Nehls, T. Farrell, and U. Scherf "Tunable organic thin-film laser pumped by an inorganic violet diode laser," Appl. Phys. Lett. 88(24), 241116 (2006).
12. S. Riechel, U. Lemmer, J. Feldmann, S. Berleb, A.G. Mückl, W. Brütting, A. Gombert, and V. Wittwer "Very compact tunable solid-state laser utilizing a thin-film organic semiconductor," Opt. Lett. 26(9), 593–5 (2001).
13. W. Zhao, T. Cao, and J.M. White. "On the origin of green emission in polyfluorene polymers: The roles of thermal oxidation degradation and crosslinking," Adv. Funct. Mater. 14(8), 783-790 (2004).
14. S. Richardson, O.P.M. Gaudin, G.A. Turnbull, and I.D.W. Samuel. "Improved operational lifetime of semiconducting polymer lasers by encapsulation," Appl. Phys. Lett. 91(26), 261104 (2007).
15. J. Herrnsdorf, B. Guilhabert, Y. Chen, A. Kanibolotsky, A. Mackintosh, R. Pethrick, P.J. Skabara, E. Gu, N. Laurand, and M.D. Dawson "Flexible blue-emitting encapsulated organic semiconductor DFB laser," Opt. Express 18(25), 25535–45 (2010).
16. A. Rose, Z. Zhu, C.F. Madigan, T.M. Swager, and V. Bulovic "Sensitivity gains in chemosensing by lasing action in organic polymers," Nature 434(April), 1–4 (2005).

17. Y. Chen, J. Herrnsdorf, B. Guilhabert, A.L. Kanibolotsky, A.R. Mackintosh, Y. Wang, R.A. Pethrick, E. Gu, G.A. Turnbull, P.J. Skabara, I.D.W. Samuel, N. Laurand, and M.D. Dawson "Laser action in a surface-structured free-standing membrane based on a π-conjugated polymer-composite," Org. Electron Elsevier B.V. 12(1), 62–9 (2011).
18. C. Foucher, B. Guilhabert, a. L. Kanibolotsky, P.J. Skabara, N. Laurand, and M.D. Dawson. "Highly-photostable and mechanically flexible all-organic semiconductor lasers," Opt. Mater. Express 3(5), 584 (2013).
19. Schott. "AF32" [Internet]. Available from: www.schott.com
20. C. Foucher, B. Guilhabert, N. Laurand, and M.D. Dawson. "Wavelength-tunable colloidal quantum dot laser on ultra-thin flexible glass," Appl. Phys. Lett. 104(14), 141108 (2014).
21. J. Chilwell, I. Hodgkinson. "Thin-films field-transfer matrix theory of planar multilayer waveguides and reflection from prism-loaded waveguides Jn," J. O. S. A. 1(7), 742–53 (1984).
22. S. Doring, M. Kolloshce, T. Rabe, J. Stumpe, and G. Kofod. "Electrically tunable polymer DFB laser," Adv. Mater. 23(37), 4265-4269 (2001).
23. A. Camposeo, P. Del Carro, L. Persano, and D. Pisignano. " Electrically tunable organic distributed feedback lasers embedding nonlinear optical molecules," Adv. Mater. 24(35), OP221-OP225 (2012).
24. A. Paint, C.H. Hare, and M.T. Section. "The degradation of coatings by ultraviolet light and electromagnetic radiation," (May) (1992).
25. L. Persano, A. Camposeo, P. Del Carro, P. Solaro, R. Cingolani, P. Boffi ,and D. Pisignano. "Rapid prototyping encapsulation for polymer light-emitting lasers, " Appl. Phys. Lett. 94 (12), 123305 (2009)
26. G. Tsiminis, Y. Wang, A. L. Kanibolotsky, A. R. Inigo, P. J. Skabara, I. D. W. Samuel, and G. A. Turnbull. "Nanoimprinted organic semiconductor laser pumped by a light-emitting diode", Adv. Mater. 25(20), 2826-2830 (2013).
27. J. Herrnsorf, Y. Wang, J. J. D. McKendry, Z. Gong, D. Massoubre, B. Guilhabert, G. Tsiminis, G. A. Turnbull, I. D. W. Samuel, Nicolas Laurand, Erdan Gu, and Martin D. Dawson. " Micro-LED pumped polymer laser: A discussion of future pump sources for organic lasers," Laser & Phot. Rev. 7 (6), 1065 (2013).

1. Introduction

Organic semiconductors (OS) are attractive for the fabrication of [1] lasers because of their broad emission spectra, high photoluminescence quantum yields and large absorption cross-sections, combined with versatility in processing which enables, for example, a wide range of bendable and mechanically-tunable devices [1–9].

Early optical pumping arrangements for OS lasers were based on relatively expensive and bulky solid-state lasers that prevented their implementation in applications. More recently, combined advances in OS laser and InGaN semiconductor technologies have led to the demonstration of OS lasers pumped by laser diodes (LD) or by light emitting diodes [10–12], paving the way for compact and low-cost OS laser systems and thereby greatly enhancing their applicability. OS lasers, however, face another hurdle to applications: photostability. Because OS materials tend to degrade in the combined presence of high-intensity light and oxygen [13], it is crucial to isolate OS lasers from air in order to increase their operational lifetime. The solution is to encapsulate the OS gain region with one or several materials that act as oxygen barriers. Such an encapsulation strategy is nevertheless difficult to achieve while maintaining the advantageous mechanical or optical properties of the device. Glass for example is an ideal encapsulation material but the resulting OS lasers so far have been mechanically rigid [14]. On the other hand, certain polymers have been used to encapsulate flexible OS lasers but they can sometimes result in a decrease in performance [15].

Here, we report a fully encapsulated mechanically flexible OS laser that circumvents the aforementioned issues by using ultra-thin glass. The demonstrated OS laser is pumped by a LD, to our knowledge the first time this has been achieved for a flexible laser, and shows improved performance in terms of threshold and photostability. In the following, section 2 explains the design and fabrication of this flexible glass laser. The optical set-up used for characterisation is also detailed, as is the multilayer slab waveguide model for the mode profile calculation, whose output is utilised in the discussion of the experimental results of section 3. The latter section presents and discusses the experimental results under 355nm

solid-state laser pumping, including wavelength tuning by bending, and under 450nm LD pumping. In particular, the substantial improvement in threshold and operation lifetime performance in comparison to an equivalent non-encapsulated laser and to other encapsulation geometries is demonstrated.

2. Design, fabrication, characterisation set-up and model

2.1 Design of the flexible/glass DFB laser and comparative laser structures

The design of the flexible glass/DFB laser is detailed in this section. Descriptions of other laser structures that were studied in order to benchmark its performance are also given.

The structure of the ultra-thin glass laser is shown in Fig. 1(a). It is formed by a 130nm-thick gain layer deposited on top of a one-dimensional grating acting as a DFB reflector. The latter is a 43µm thick epoxy layer with the nanopattern on its surface. The gain layer is a neat OS, π–conjugated poly[2,5-bis(2',5'-bis(2"-ethylhexyloxy)phenyl)-p-phenylene vinylene] (BBEHP-PPV). The gain spectrum of BBEHP-PPV spans the 490-540nm region while the absorption peaks at 431 nm [16,17]. This gain material is overcoated with a 180nm-thick layer of Polyvinyl alcohol **(**PVA). Additionally, the overall laser cavity is encapsulated between two identical 30µm-thick flexible glass sheets. The role of the PVA layer is two-fold: (i) it acts as a first oxygen barrier and (ii) it protects the OS surface integrity during addition of the flexible glass. The thickness of this PVA layer was chosen for optimum threshold performance as explained in section 3.

The comparative laser structures with no flexible glass are also represented in Fig. 1 and described hereafter. The so-called 'neat laser' [Fig. 1(b)] is simply made of a 130nm layer of BBEHP-PPV deposited on top of the epoxy grating. In this case, there is an acetate sheet below the epoxy for ease-of-handling. The other laser structure [Fig. 1(c)] is similar but includes a 180nm thick PVA layer on top the gain region. In the rest of the paper, for conciseness, these different laser structures are referred to as: "the flexible glass laser", "the neat laser" and "the PVA laser" respectively.

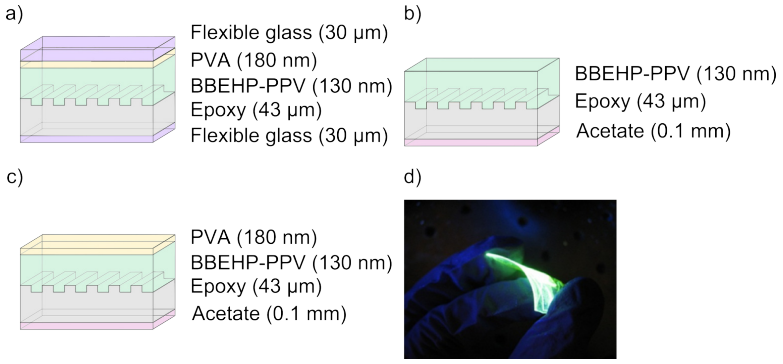

Fig. 1: Schematics of the device structures: (a) encapsulated laser overcoated with a 180nm thick layer of PVA and sandwiched between two ultra-thin flexible glass membranes, (b) neat BBEHP-PPV laser and (c) encapsulated laser with a layer of PVA (180nm). (d) a photo of a BBEHP-PPV laser encapsulated with glass and PVA under UV exposure showing bendability

2.2 Fabrication steps

The epoxy grating is identical for all lasers. It is made by soft lithography using a glass master grating with a 350nm period, following the fabrication process described in [18]. For the flexible glass laser, once the replicated grating has been post-cured, it is removed from the

acetate substrate. The resulting 43µm-thick free-standing epoxy grating is then transferred onto a 30µm thin-glass membrane (AF 32 thin glass from Schott) [19,20]. A drop of NOA65 is spin-coated at 8000 rpm on top of the 30µm-thick flexible glass substrate prior to this transfer. The latter is followed by a photocuring step under UV flooding for a total exposure dose of 300 mJ/cm^2. For all lasers, a solution of BBEHP-PPV in toluene at 20 mg/mL is spin-coated on top of the epoxy grating to form the gain layer. Then, in the case of the PVA and flexible glass laser structures, a solution of PVA in D.I. water (50 mg/mL) is spin-coated on top of the gain medium in order to form a 180nm layer. The flexible laser necessitates an additional step: a second ultra-thin glass membrane is deposited on top of the device. NOA65 is used to seal the edges of the two glass membranes together. A final photocuring step is applied (UV dose of 300 mJ/cm^2). Finally, the samples are annealed at 35°C for three days to evaporate the solvent in the PVA layer and favour its good crystallisation. Each laser was fabricated in air.

As shown in figure 1(d), the flexible glass laser is readily bendable, thanks to the total device thickness being less than 105 µm.

2.3 Laser characterisation set-ups

All lasers were first assessed under 355nm solid-state laser pumping (5ns pulses at 10 Hz). The full width at half maximum (FWHM) pump stripe size on the sample under test was 1.789 x 0.329 mm^2, as measured by knife edge. For each laser, the power transfer function, spectra and photostability were measured. For the latter, in order to determine the operating lifetime, the intensity of each laser was monitored and recorded every thirty seconds (i.e. every ~300 pulses) when operated above threshold, at a pump fluence of 0.59 mJ/cm^2. The degradation dosage, F_{deg}, is defined as the total pumping dosage for which the laser intensity drops to 1/e of its initial value.

To study the effect of mechanical bending on the emission wavelength of the flexible glass laser, the same method as in [20] was used, see Fig. 5(a). The laser was fixed on a special holder that enabled bending of the flexible glass. The radius of curvature could be made either negative or positive as seen in Figs. 5(b) and 5(c), respectively increasing or decreasing the grating period, and in turn inducing a red shift or a blue shift of the laser wavelength.

Diode pumping experiments were made with an InGaN laser diode (LD) emitting at 450 nm, its beam focussed on the DFB laser to a spot of 390 x 220 µm^2. The LD delivers nanosecond pulses with energies up to 150 nJ at a repetition rate of 10 Hz. It is driven by a high voltage power supply coupled to a PCB driving board (PCO-7110). The optical characteristics of the LD are plotted in figure 2, showing the pulse width and the fluence as a function of the driving peak current. F_{deg} of the lasers under LD pumping was measured at a pump energy fluence of 27 µJ/cm^2 and at a frequency of 10 Hz.

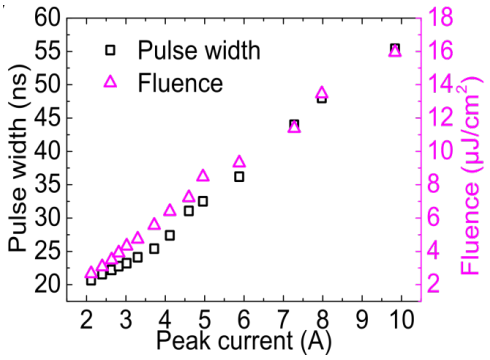

Fig. 2: LD optical pulse fluence and duration plotted against the driving peak current

2.4 Mode profile

For the discussion on the threshold performance in section 3, the laser mode transverse intensity profile and its overlap with the gain region are calculated for the different types of laser structures. This overlap, characterised by the overlap factor [Eq. (1)], is important because it influences the modal gain and hence the laser threshold: a higher overlap factor leading in principal to a lower threshold.

$$\frac{\int_{active\_region} I(z).dz}{\int_{-\infty}^{+\infty} I(z).dz} \qquad \text{Eq. (1)}$$

The matrix-based model that was used for this considers the laser structure as a multilayer slab waveguide [18,21]. In the case of the neat laser there is only one layer to be considered, the gain material BBEHP-PPV, refractive index n~1.7, enclosed between the epoxy substrate (NOA65), n~1.52 and considered semi-infinite, and the air medium. For the PVA laser, the additional PVA layer, n~1.55, has to be taken into account [18]. For the flexible glass lasers, the different sections include the ultra-thin glass substrate (n~1.51), the epoxy layer, the BBEHP-PPV layer, the PVA thin film and the top thin glass membrane. The calculated mode and refractive index profiles of the neat laser and of the PVA lasers are plotted in Fig. 3 as examples. The modal effective refractive index was also determined with this model. Table 1 summarises the values of the overlap factor and the modal effective refractive index for each laser structure.

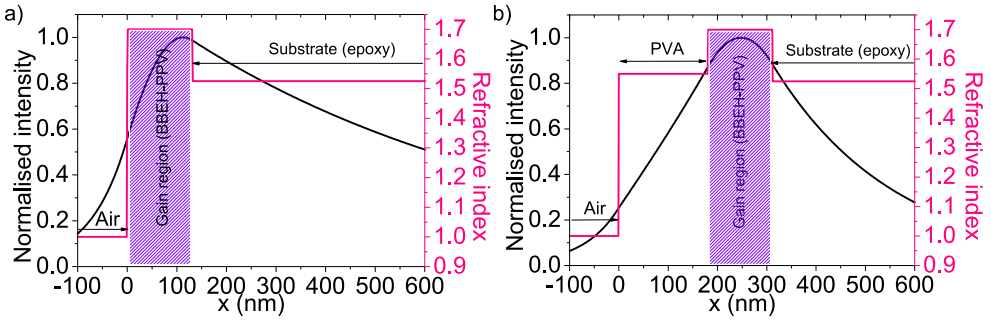

Fig. 3: Mode profile superposed onto the refractive index profile of the multilayer structure for (a) a neat laser and (b) a laser encapsulated with a 180nm PVA layer. The region of overlap with the gain layer is highlighted.

Table 1: Values of the overlap and effective refractive index for each laser

Material	Overlap (%)	n_{eff}
Neat	12.0	1.53
180nm thick PVA	29.5	1.56
Glass + 180nm thick PVA	26.5	1.57

3. Experimental results and discussions

3.1. 355nm pumping

3.1.1 Laser characteristics

The performance of each laser is plotted in Figure 4, where Fig. 4(a) represents the emission spectra above threshold and Fig. 4(b) the laser transfer functions.

The neat laser is used as the main reference for performance comparison. It emits at 536.9 nm. The difference with the expected wavelength (as determined from the n_{eff} value in Table 1) is caused by the repeatability limits of film deposition during fabrication as well as by uncertainties in the materials refractive indices. The average threshold energy fluence, F_{th}, is found to be 239.5 μJ/cm^2 per pulse (corresponding to a power density threshold of 47.9 kW/cm^2). The degradation dosage, F_{deg}, of this neat laser is 5.8 J/cm^2 (data not shown).

The emission wavelength of the PVA encapsulated laser is 537.8 nm. The average threshold is 8.0 μJ/cm^2 (1600 W/cm^2). These values show that the overcoated PVA layer both redshifts the oscillation wavelength and lowers the threshold. These effects are mainly due to changes in the refractive index profile of the laser structure as shown in Figure 3. As a result of the PVA layer addition, the laser mode is pulled away from the substrate and overlaps more with the gain region leading to an increase in the effective refractive index of the mode, hence a longer oscillating wavelength. As shown in section 3, the overlap factor is 12.0% for the neat laser and 29.5% for the PVA laser encapsulated. This is consistent with the trend in threshold observed experimentally. We note that there is an optimum PVA thickness (close to 190 nm) however. For example, if the PVA thickness is increased to 580 nm, the overlap factor decreases to 26% and the threshold increases to 13.0 μJ/cm^2 (2600 W/cm^2). F_{deg} is found to be 46.6 J/cm^2 [Fig. 6(b)] for the 180-nm PVA layer, i.e. 8 times longer than for the neat laser. The dominant degradation is assumed here to come from molecular oxygen diffusing from the environment into the gain layer. The PVA slows down this diffusion resulting in the improvement in operation lifetime for the PVA laser. F_{deg} is even higher for a 580-nm PVA layer at 390 J/cm^2, which is ~68 times that of the neat BBEHP-PPV laser. However, a 180nm thickness was chosen in our laser design as a trade-off between threshold performance and oxygen barrier function.

The emission wavelength of the ultra-thin glass laser is 537.1 nm. The average threshold fluence is measured to be 10.8 μJ/cm^2, i.e. a 22-fold improvement in threshold compared to the equivalent neat laser. However, it is slightly higher than the PVA laser. Again this can be explained by the overlap factors, 26.5% for the PVA laser versus 24.1% for the flexible glass laser (see Table 1).

F_{deg} is 681 J/cm^2 [Fig. 7(b)] which is ~14.6 times higher than for the PVA laser and 118 times higher than for the neat laser. This result shows that, as expected, the glass encapsulation further protects the gain material. We note that the pump energy fluence F_{deg} of the flexible glass laser increases only marginally to 701 J/cm^2 if the PVA thickness is

increased to 580 nm. This shows that the flexible glass is the main contributor to the long device photostability.

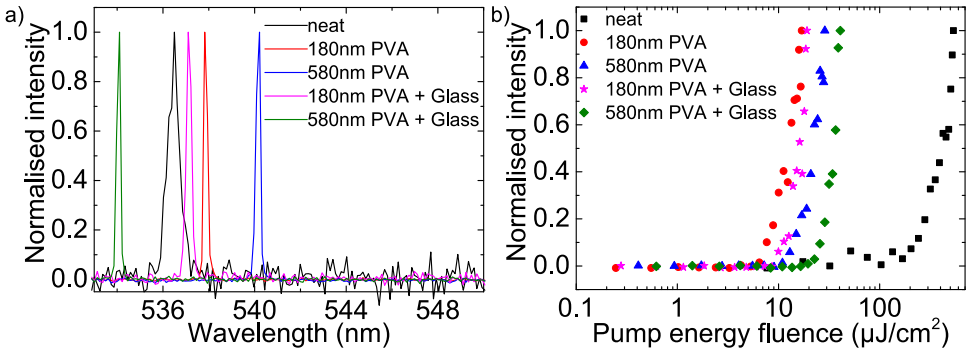

Fig. 4: (a) shows the emission spectra and (b) represents the power transfer functions of each laser when pumped at 355 nm

3.1.2 Wavelength tunability by bending

Organic DFB lasers can be tuned by coupling them to electroactive polymers for example [22,23], but also by mechanical bending if the laser is flexible [20]. The behaviour of the flexible glass laser when bending the glass is studied. The emission wavelength above threshold for different bending radii of curvature is shown in figure 5. For these measurements, the pump energy is kept constant at 1.68 μJ. Reducing the radii of curvature to -1.9 and -1.7 cm induces a blue shift of the wavelength by 2.2 nm and 4.8 nm, respectively. For radii of curvature of +1.8 and +1.0 cm, the wavelength red-shifts by 2.1 nm and 4.6 nm, respectively. The total tuning of 9.4 nm is limited by the maximum radius of curvature before fracture of the device and not the gain bandwidth of the gain material. A radius of curvature inferior to 1.0 cm engenders an irreversible degradation of the sample.

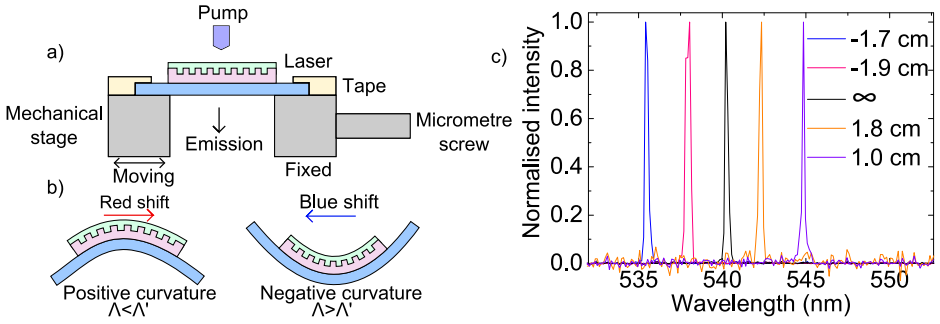

Fig. 5: (a) Schematics of the set-up for testing mechanical bending of ultrathin glass laser with 180nm PVA overcoat, (b) the two ways the laser can be bent, increasing or reducing the grating period for, respectively, red shifting or blue shifting the laser emission wavelength and (c) shift in the emission wavelength of the flexible encapsulated DFB laser with glass for different radii of curvature.

3.2. 450nm LD pumping

3.2.1 PVA laser

Figure 6 shows the characteristics of the PVA laser when pumped with the 450nm LD. The laser emits at 537.6 nm wavelength as seen in inset of Fig. 6(a), with a <0.20nm linewidth. This shows that the pump wavelength has no significant effect on the oscillating wavelength of the OS laser. The average pump threshold of the device is 11.1 μJ/cm^2, corresponding to a LD power density at threshold of ~269 W/cm^2 [Fig 6(a)]. This is about 6-times lower than the power density threshold when pumping at 355 nm and is attributed to the higher absorption (about 2 times higher) of BBEHP-PPV at 450 nm [17]. For information, LED-pumped lasers fabricated by nanoimprint have been reported with 770W/cm^2 threshold for a second order grating [26] and as low as 197 W/cm^2 for mixed-order gratings [27].

The intensity decays of the device due to photodegradation when pumped by the LD at 450 nm and by the solid-state laser at 355 nm are plotted in fig. 6(b). A pump energy fluence for degradation F_{deg} of 88.0 J/cm^2 is found when pumping at 450nm, representing an operating lifetime ~2-times longer than when pumping at 355 nm. This increase in photostability could be explained by the longer wavelength of the LD, giving a lower quantum defect and lower energy photons as UV radiation is known to damage organic molecules by breaking covalent bonds [24].

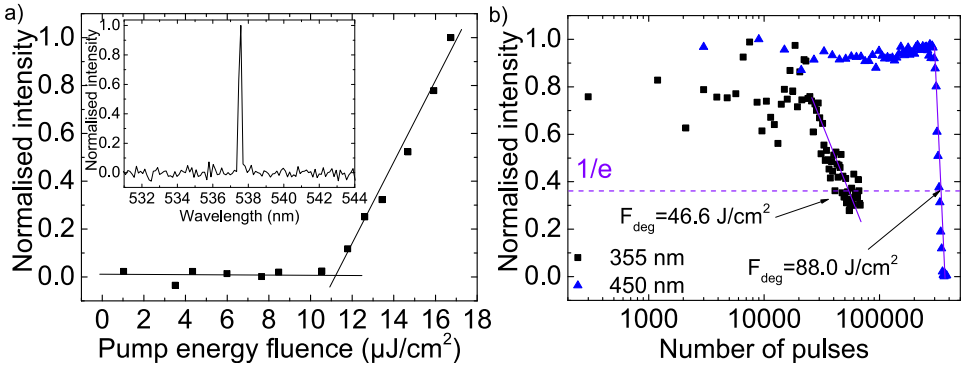

Fig. 6: (a) spectrum and power transfer function of the 180nm PVA encapsulated BBEHP-PPV laser and b) its intensity decay caused by photodegradation when pumped at 355 nm (black squares) and at 450 nm (blue triangles) (the x axis has a logarithm scale)

3.2.2 Ultrathin glass laser

The power transfer function and the spectrum above threshold of the LD-pumped ultra-thin glass laser are plotted in Fig. 7(a). The laser emits at 540.4 nm wavelength (inset) with a <0.16nm linewidth and a LD power density at threshold of ~290 W/cm^2 (14 μJ/cm^2), corresponding to a 7-time improvement in threshold compared to the device pumped at 355 nm. Again, this is due to the higher absorption of BBEHP-PPV at 450 nm.

Fig. 7(b) shows the photostability of the laser when pumped with the LD at 450 nm and with the solid-state laser at 355 nm. As seen for the PVA laser, F_{deg} presents a ~2-fold improvement compared to a similar device pumped in the UV, i.e. F_{deg} of 1440 J/cm^2 compared to 681 J/cm^2 when pumping at 355 nm. This confirms the influence of the lower quantum defect and UV radiation on organic compounds. The degradation of the laser could

be partly attributed to oxygen trapped inside the different layers of the laser during the fabrication process.

This degradation dosage is ~40 times higher than for the resin encapsulation format reported in [25]. An OS DFB laser encapsulated with thick glass, reported in [14], had a value of ~10^6 J/cm^2, which is ~ 700 times higher. We note though that in these studies the pumping conditions are different, as are the gain materials. Such parameters all have an effect on device operating lifetime irrespective of the encapsulating format. Nevertheless, this present paper reports what we believe to be the longest photostability for a bendable OS laser. The LD pulses are longer than the 355nm pump (70 ns versus 5 ns). The photoluminescence lifetime of BBEHP-PPV is typically below 0.5 ns. It is possible that the pulse duration has an effect on the photostability result. If this is the case, then this makes the positive effect of thin-glass encapsulation even more pronounced. Overall, the LD-pumped thin-glass laser combines the best-combined performance in terms of threshold and photostability.

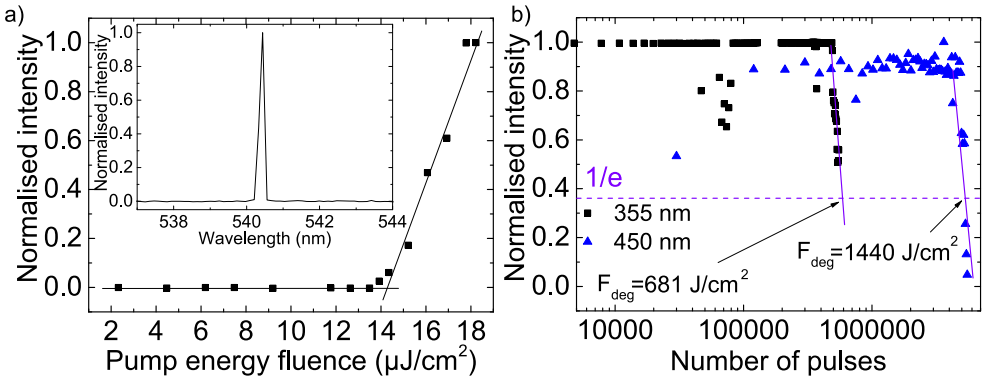

Fig. 7: (a) spectrum and power transfer functions of the encapsulated BBEHP-PPV lasers with a layer of PVA of 180 nm and glass and (b) its intensity decay when pumped at 355 nm (black squares) and at 450 nm (blue triangles) (the x axis has a logarithm scale)

Table 2 summarises the main results of this study.

Table 2: Summary of the results on neat and encapsulated lasers

Characteristics		Laser		
		Neat	*180nm thick PVA*	*Glass + 180nm thick PVA*
Wavelength (nm)		536.9	537.8	537.1
Fluence Threshold (μJ/cm^2)	Laser pumping	239.5	8.0	10.8
	LD pumping	X	11	14
Power density threshold (W/cm^2)	Laser pumping	47900	1600	2160
	LD pumping	X	269	290
F_{deg} (J/cm^2)	Laser pumping	5.8	46.6	681
	LD pumping	X	88.0	1440

4. Conclusion

LD pumped mechanically-flexible OS lasers fully encapsulated with PVA and ultra-thin glass membranes are demonstrated. These lasers show combined improvement in operation lifetime (up to 250 times) and in power density threshold performance (up to 265-time reduction) over the equivalent non-encapsulated device. This demonstration brings OS lasers closer to applications. The combination of a mechanically-flexible laser cavity with a laser-diode for pumping and the achievement of high photostability offer a potential solution for low-cost, compact systems suitable for (bio)-sensing, medical diagnostics and spectroscopy.

Acknowledgments

This work was supported by the EPSRC grant EP/J021962/1 “Hybrid Colloidal Quantum Dot Lasers for Conformable Photonics”. The authors also wish to acknowledge A. L. Kanibolotsky and P. J. Skabara for synthesizing BBEHP-PPV.